AGU PUBLICATIONS

Geophysical Research Letters

RESEARCH LETTER
10.1002/2014GL059378

Key Points:
- Density and porosity structure within the lunar crust was quantified
- The porosity is eliminated at 10-20 km depth due to lithostatic pressure
- Improved lunar crustal gravity models were constructed

Correspondence to:
S.-C. Han,
shin-chan.han@nasa.gov

Citation:
Han, S.-C., N. Schmerr, G. Neumann, and S. Holmes (2014), Global characteristics of porosity and density stratification within the lunar crust from GRAIL gravity and Lunar Orbiter Laser Altimeter topography data, *Geophys. Res. Lett., 41*, 1882–1889, doi:10.1002/2014GL059378.

Received 21 JAN 2014
Accepted 28 FEB 2014
Accepted article online 4 MAR 2014
Published online 26 MAR 2014

Global characteristics of porosity and density stratification within the lunar crust from GRAIL gravity and Lunar Orbiter Laser Altimeter topography data

Shin-Chan Han[1], Nicholas Schmerr[1,2], Gregory Neumann[1], and Simon Holmes[1,3]

[1]Planetary Geodynamics Laboratory, NASA Goddard Space Flight Center, Greenbelt, Maryland, USA, [2]Department of Geology, University of Maryland, College Park, Maryland, USA, [3]SGT, Inc., Greenbelt, Maryland, USA

Abstract The Gravity Recovery and Interior Laboratory (GRAIL) mission is providing unprecedentedly high-resolution gravity data. The gravity signal in relation to topography decreases from 100 km to 30 km wavelength, equivalent to a uniform crustal density of 2450 kg/m^3 that is 100 kg/m^3 smaller than the density required at 100 km. To explain such frequency-dependent behavior, we introduce rock compaction models under lithostatic pressure that yield radially stratified porosity (and thus density) and examine the depth extent of porosity. Our modeling and analysis support the assertion that the crustal density must vary from surface to deep crust by up to 500 kg/m^3. We found that the surface density of megaregolith is around 2400 kg/m^3 with an initial porosity of 10–20%, and this porosity is eliminated at 10–20 km depth due to lithostatic overburden pressure. Our stratified density models provide improved fits to both GRAIL primary and extended mission data.

1. Introduction

The thickness and structure of the lunar crust are key constraints on bulk composition, evolution, and formation of the Moon. Over the past 4.5 billion years, the primarily anorthositic lunar crust has been modified by mare volcanism and extensive impact cratering into layers of surface regolith and megaregolith, underlain by fractured and faulted crustal rock [*Töksoz et al.*, 1974; *Hartmann*, 1973]. The in situ Apollo Passive Seismic Experiment observations of crustal elastic properties revealed that the megaregolith is between 1 and 3 km thick [*Töksoz et al.*, 1974; *Nakamura*, 2011]. Megaregolith consists of poorly consolidated ejecta fragments and brecciated crustal materials, and is expected to contain large amounts of granular pore space that gives rise to lowered densities. The majority of this pore space would be eliminated by viscous deformation and compaction of crustal materials [*Wieczorek et al.*, 2013a]. This implies a stratified density structure in the lunar crust, with the lower crustal density closer to anorthosite (2800–2900 kg/m^3). Determination of this layering is essential for improving gravitational models of the lithosphere and crustal thickness and for quantifying and understanding the mechanical property of the lunar crust.

Remote sensing of lunar crustal thickness, density, and layering is made possible through gravity and topography measurements. They reveal that lunar crustal thickness is highly variable, ranging from 1 to 60 km in thickness [*Wieczorek et al.*, 2013a]. New gravity data obtained by the Gravity Recovery and Interior Laboratory (GRAIL) mission are providing unprecedentedly high-resolution maps that are enabling detailed regional mapping of bulk density, porosity, and thickness of the crust [*Zuber et al.*, 2013]. Preliminary results for variation in bulk crustal densities from GRAIL by *Wieczorek et al.* [2013a] are on the order of 2550 ± 250 kg/m^3, considerably less than the 2800–2900 kg/m^3 expected for typical anorthositic materials. Furthermore, *Han* [2013] estimated even lower density from the higher-frequency gravity data. *Wieczorek et al.* [2013a] determined regionally varying densities that are consistent with 4–21% porosity within the entire lunar crust. However, extensive impact gardening would increase porosity primarily within the shallow megaregolith layer, not uniformly.

Examination of the spectral response between gravity and topography may reveal the density stratification structure. Figure 1 shows the observed correlation and admittance spectra between the GRAIL gravity field [*Konopliv et al.*, 2013; *Lemoine et al.*, 2013] and the synthetic gravity models computed from Lunar Orbiter Laser Altimeter (LOLA) topography data [*Smith et al.*, 2010]. The synthetic gravity model was computed with a

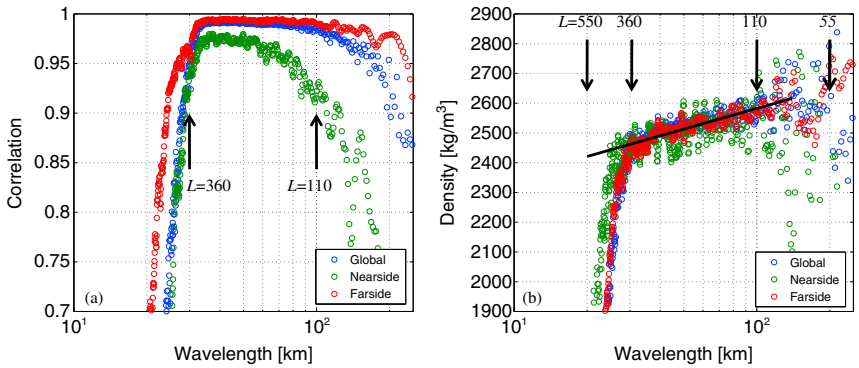

Figure 1. (a) Correlation and (b) admittance spectrum between the GRAIL gravity field and the synthetic gravity model computed from LOLA topography using the unit density. The wavelength λ and spherical harmonic degree l is related via $\lambda = 11,000$ km/l, where 11,000 km is the circumference of the Moon. They are shown globally and over the nearside and the farside, separately.

nominal density applied uniformly throughout the crust, and the admittance spectrum was scaled by that uniform density. The correlation and admittance spectra were computed globally and over the nearside and farside separately by applying the spatial localization window [*Wieczorek*, 2008]. The correlation is near unity for wavelengths of 30–100 km (spherical harmonic degrees, $l = 110$–360). The lowered correlations at shorter wavelengths ($<$ 30 km) are due to the reduced gravity signal at the primary mission mean altitude (55 km), while those at longer wavelengths ($>$ 100 km) are likely due to geophysical processes such as lithospheric flexure and mantle heterogeneity. There is a slightly higher and lower correlation than the global average found for the farside and nearside, respectively. The near unity spectral correlation over the wavelengths of 30–100 km suggests a primarily topographic contribution to the gravity field. The observed admittance decreases at shorter wavelengths; 2550–2600 kg/m^3 at 100 km ($l = 110$) and 2450 kg/m^3 at 30 km ($l = 360$), which is difficult to explain with a uniform density model.

In this study, we examine the hypothesis that the megaregolithic pore space is removed with increasing overburden pressure at depth, and that the resulting stratified density with depth is responsible for such frequency dependence found in the admittance spectrum. We introduce a simple, experimental model for rock compaction with pressure (i.e., depth) to describe the general characteristic of the lunar crust and examine the corresponding gravity response. Finally, we obtain the global description of crustal density stratification from the GRAIL gravity and LOLA topography data.

2. A Model for Density, Porosity, and Compaction

The increase of lithostatic pressure with depth closes pores and fractures within the megaregolith, leading to a gradual decrease in lunar crustal porosity with depth [*Keihm and Langseth*, 1977]. Compaction profiles of porosity as a function of depth are dependent upon the material properties of the sediments and pore fluids involved [*Sclater and Christie*, 1980], though on the Moon, the effect of pore fluids can be reasonably neglected. The removal of porosity with depth has been described for terrestrial sediments using simple exponential functions that relate the change in porosity with depth (generalized to pressure) for compaction of a given material [e.g., *Athy*, 1930; *Audet and Fowler*, 1992]:

$$\phi(r) = \phi_1 \exp(-cP(r)/P_c), \tag{1a}$$

$$\rho(r) = \rho_0(1 - \phi(r)), \tag{1b}$$

where c is a constant (~6.15), ρ_0 is grain density (zero porosity), ϕ_1 is the surface porosity, $P = P(r)$ is the lithostatic overburden pressure, and P_c is the characteristic closure pressure of the material; both porosity ϕ and starting porosity ϕ_1 are percentages divided by 100. The value of c and P_c (MPa) are related to an experimentally derived pressure for which the porosity falls below 0.2% for a material [*Sclater and Christie*, 1980]. They describe the pressure at which the pore space is effectively eliminated within a rock and can vary widely across different rock types (Figure 2). The density distribution with depth is described by

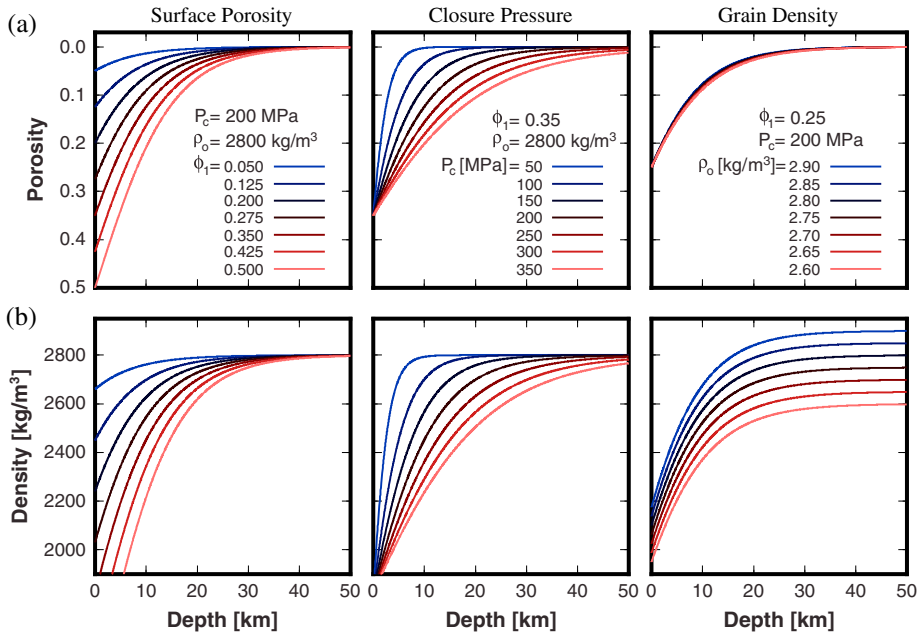

Figure 2. Depth variation in theoretical lunar crustal structures for (a) porosity and (b) the associated density. Model space parameters include surface porosity ϕ_1, closure pressure P_c, and grain density ρ_0. Porosity is assumed to be vacuum, while grains are anorthosite. In each panel, two parameters are held fixed while the third is allowed to vary. Depth (z) is converted from lithostatic pressure using $z = \sum_{i=0}^{n} \Delta P/\rho_i g$, where ΔP is the pressure increment (MPa), n the number of pressure increments, and $g = 1.67$ m/s^2.

equation (1b), where $\rho_1 = \rho_0(1 - \phi_1)$ is the surface density. The pore space of lunar materials is assumed to be vacuum with null density.

Figure 2 illustrates the relationship between porosity and density distribution with depth for depth-dependent porosity models with differing cases of surface porosity ϕ_1, closure pressure P_c, and grain density ρ_0. In our modeling, we explore a range of porosities (0.0–0.8) at pressures appropriate for the lunar crust (0–400 MPa) and grain densities (2600–2900 kg/m^3). In general, models with low P_c result in steep porosity gradients across the crust, which are further steepened at higher surface porosities. Models with high P_c produce more gradual porosity gradients, as does reducing the surface porosity. Finally, Figure 2 demonstrates that the porosity distribution over depth is largely independent of the unperturbed grain density. The model does not explicitly include temperature dependent viscosity and grain boundary annealing, effects that would reduce porosity [*Wieczorek et al.*, 2013a]. Instead of specifying a particular value of P_c, we allow the parameter to vary freely. A reduction in crustal porosity resulting from these mechanisms would tend to reduce compaction depth and would thus be fit with a lower P_c.

3. Admittance Model of Stratified Density

The gravity anomaly from the deeper layer attenuates faster than that from the shallower layer, and, as a result, the shorter wavelength components of the observed gravity at the surface are biased toward the shallower layer. This makes it possible to reveal the density stratification from the spectral response such as admittance between gravity and topography. In this section, we derive the analytic expression of the theoretical admittance spectrum for a stratified density structure. The spherical harmonic coefficients of the gravitational potential anomaly due to the topography anomaly are obtained, to the first order, as [*Turcotte et al.*, 1981]

$$C^0_{ilm} = \frac{4\pi a^3}{M(2l+1)} \rho^0 \left(\frac{h_{ilm}}{r_1}\right) \left(\frac{r_1}{a}\right)^{l+3}, \tag{2}$$

where we followed the convention of spherical harmonic expansion in *Wieczorek and Phillips* [1998] for the coefficients of topography h_{ilm} and of gravitational potential C^0_{ilm}. The radius, a, where we evaluate the potential is 1738 km. The mean radius of the topography is r_1 and the nominal crustal density is ρ^0.

For models consisting of N discrete layers with different densities varying only in depth (or radius), the topography anomaly at each density interface produces the additional gravity anomalies, to the first order, as follows:

$$C_{ilm} = \frac{4\pi a^3}{M(2l+1)} \sum_{k=1}^{N} \Delta\rho_k \left(\frac{h_{ilm}}{r_k}\right)\left(\frac{r_k}{a}\right)^{l+3}, \tag{3}$$

where $\Delta\rho_k$ is the density contrast ($\rho_k - \rho_{k-1}$) at the kth interface that is expanded with the same topography coefficients h_{ilm} but referring to the mean radius r_k. Here $r_k < r_{k-1}$ and $\Delta\rho_1$ are the density of the topmost layer referred to the mean radius r_1 = 1737.151 km for the Moon.

The correlation spectrum between two coefficients C_{ilm} and C^0_{ilm}, $\frac{\sum_{i,m} C_{ilm}C^0_{ilm}}{\sqrt{\sum_{i,m} C^0_{ilm}C^0_{ilm}}\sqrt{\sum_{i,m} C_{ilm}C_{ilm}}}$, can be readily verified to be unity, because each density interface is parallel to the surface topography. The admittance spectrum, $\frac{\sum_{i,m} C_{ilm}C^0_{ilm}}{\sum_{i,m} C^0_{ilm}C^0_{ilm}}$, is computed to be $\sum_{k=1} \frac{\Delta\rho_k}{\rho^0}\left(\frac{r_k}{r_1}\right)^{l+2}$. It becomes a constant $\frac{\Delta\rho_1}{\rho^0}$ if there is no density variation with depth. Therefore, the "density" admittance spectrum (scaled by ρ^0), defined as $\gamma_l \equiv \rho^0 \left(\frac{\sum_{i,m} C_{ilm}C^0_{ilm}}{\sum_{i,m} C^0_{ilm}C^0_{ilm}}\right)$, is written as

$$\gamma_l = \sum_{k=1} \Delta\rho_k \left(\frac{r_k}{r_1}\right)^{l+2}. \tag{4}$$

Equations (2) and (3) are accurate only to a first-order approximation in computing gravitational potential from topography. The effect of finite amplitude of topography must be considered. Equation (4), however, is sufficient to compute the theoretical admittance spectrum given the density variation with radius. We numerically verified the accuracy of equation (4) by computing the gravitational potential coefficients of C^0_{ilm} and C_{ilm} in two different ways: (i) considering the higher-order terms to account for the effect of finite amplitude topography [*Wieczorek and Phillips*, 1998] and (ii) numerically integrating spherical prisms (tesseroid) with the dimension of ~1 km in latitude, longitude, and radius [*Heck and Seitz*, 2007]. Then, we computed two sets of the admittance spectrum from those coefficients of C^0_{ilm} and C_{ilm}, and compared them with equation (4). For most cases of stratification, the density admittance spectrum γ_l can be computed directly using equation (4) with the relative error of less than 0.1%.

Figure 3a shows four examples of depth-dependent density models with various cases of surface porosity ϕ_1, closure pressure P_c, and grain density ρ_0. The corresponding admittance spectrum for each density model was computed from the analytical approach using equation (4) and from two numerical approaches (finite amplitude and tesseroid integration) and shown in Figure 3b. The result from the numerical tesseroid integration slightly differs from the analytical one, particularly for shorter wavelengths (< 10 km). It is because the thickness of the tesseroid was fixed to 1 km for computational efficiency, while the layer was discretized every 0.1 km for the analytical approach. Over the wavelengths of 30–100 km, it is found that the admittance spectra decrease almost linearly as wavelength decreases. They asymptotically converge to the grain density ρ_0 at the longest wavelength and the surface density $\rho_1 = \rho_0(1 - \phi_1)$ at the shortest wavelength. The admittance spectrum is sensitive to all three model parameters, ρ_0, ϕ_1, and P_c.

4. Result From GRAIL Gravity Data

In this section, we quantify the density stratification within the bulk lunar crust from the GRAIL observation of global gravity field. For our global analysis, it is assumed that the density changes only with overburden pressure (i.e., depth); and therefore, the shape of each density interface is modeled using the LOLA surface topography. We examined a number of different cases of radial density and porosity stratification by changing three model parameters of ϕ_1 (0.025–0.800), P_c (25–500 MPa), and ρ_0 (2600–2900 kg/m^3). For all cases, the computed gravitational potential models yield near unity correlation with the potential model of the uniform density. For each case, we calculated the theoretical admittance spectrum (equation (4)) and

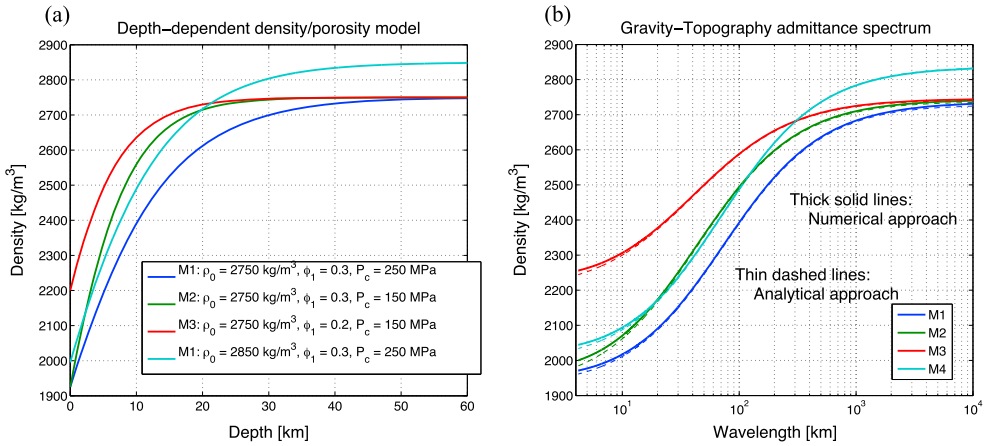

Figure 3. (a) Depth-density model after *Athy* [1930] based on an experimental relationship between overburden pressure and porosity. As in Figure 2, ρ_0, ϕ_1, and P_c are the three control parameters to determine the density stratification within the crust. (b) The theoretical admittance spectrum corresponding to each of the density stratification models is shown in Figure 3a. The dashed lines are from the analytic relationship given in equation (4), and the solid lines are from the numerical computation.

compared with the observed admittance spectrum (Figure 1b). We used the admittance observation along with its uncertainty only over wavelengths of 30–100 km ($l = 110$–360), where near unity correlation is obtained.

In order to quantify the agreement between the model and observation, we calculated the reduced chi-squared statistic defined as $\chi_r^2 = \frac{1}{D}\sum_{l=L1}^{L2} \frac{\left(\gamma_l^{\mathrm{obs}} - \gamma_l^m\right)^2}{\sigma_l^2}$, where γ_l^{obs} is the observed admittance with its variance σ_l^2 computed using equation (7) of *Wieczorek* [2008], γ_l^m is the theoretical admittance given from a density model (equation (4)), and D is the degree of freedom ($L2 - L1 - 2$, $L2 = 360$, and $L1 = 110$). Figure 4a presents the reduced chi-squared statistic for various ϕ_1 and P_c with ρ_0 of 2650, 2750, and 2850 kg/m^3, respectively. The density models that fit the GRAIL admittance spectrum within its uncertainty of 25 kg/m^3 are found from $\chi_r^2 < 2$. Those best fit models are shown, in terms of a depth-density relationship, in Figure 4b, as dashed lines with different colors for different ρ_0. The corresponding theoretical admittance spectra are presented in Figure 4c, along with the GRAIL observation.

In general, as ρ_0 increases, ϕ_1 increases such that surface density $\rho_0(1 - \phi_1)$ approaches to 2300–2400 kg/m^3. The closure pressure P_c (inferring a thickness of porous layer) trades off with ϕ_1 particularly when ρ_0 is smaller. For smaller ρ_0, the following two types of density stratification are found: (1) a thinner and highly porous layer concentrated at the top few kilometer with rapid density increase with depth and (2) gradually increasing density to a depth of 10–20 km. As ρ_0 increases, the first model type is statistically ruled out, and the solutions converge to the second case, i.e., the porosity spread over a few tens of kilometer from the surface, as highlighted in Figure 4b with thick solid lines. As shown in Figure 4c, all of the models fit the GRAIL data within the chosen bandwidth (wavelengths of 30–100 km) and diverge at shorter wavelengths (< 30 km). The GRAIL extended mission (XM) gravity data may discriminate further among the differences in these models at shorter wavelengths.

The geophysical process reduces the correlation of gravity with topography at longer wavelengths (> 100 km) and so does the reduced sensitivity of GRAIL measurements at shorter wavelengths (< 30 km), as shown in the free-air coherence (squared correlation) spectrum of Figure 5a. We also computed the Bouguer gravity anomaly by subtracting the computed gravity models from the GRAIL gravity field data. The Bouguer anomaly ideally infers the interior (other than crust) processes at longer wavelengths and any mismodeled crustal processes, as well as the gravity data noise at shorter wavelengths. *Wieczorek et al.* [2013a] and *Han* [2013] found that the bulk crustal density of 2550 kg/m^3 minimizes the Bouguer coherence spectrum over the bandwidth of 30–100 km. However, Figure 5a presents that the Bouguer coherence spectrum with the uniform density systematically increases from 50 to 30 km while the free-air coherence stays close to unity. The excessive increase in the Bouguer coherence and the decrease in the free-air coherence from 30 km to

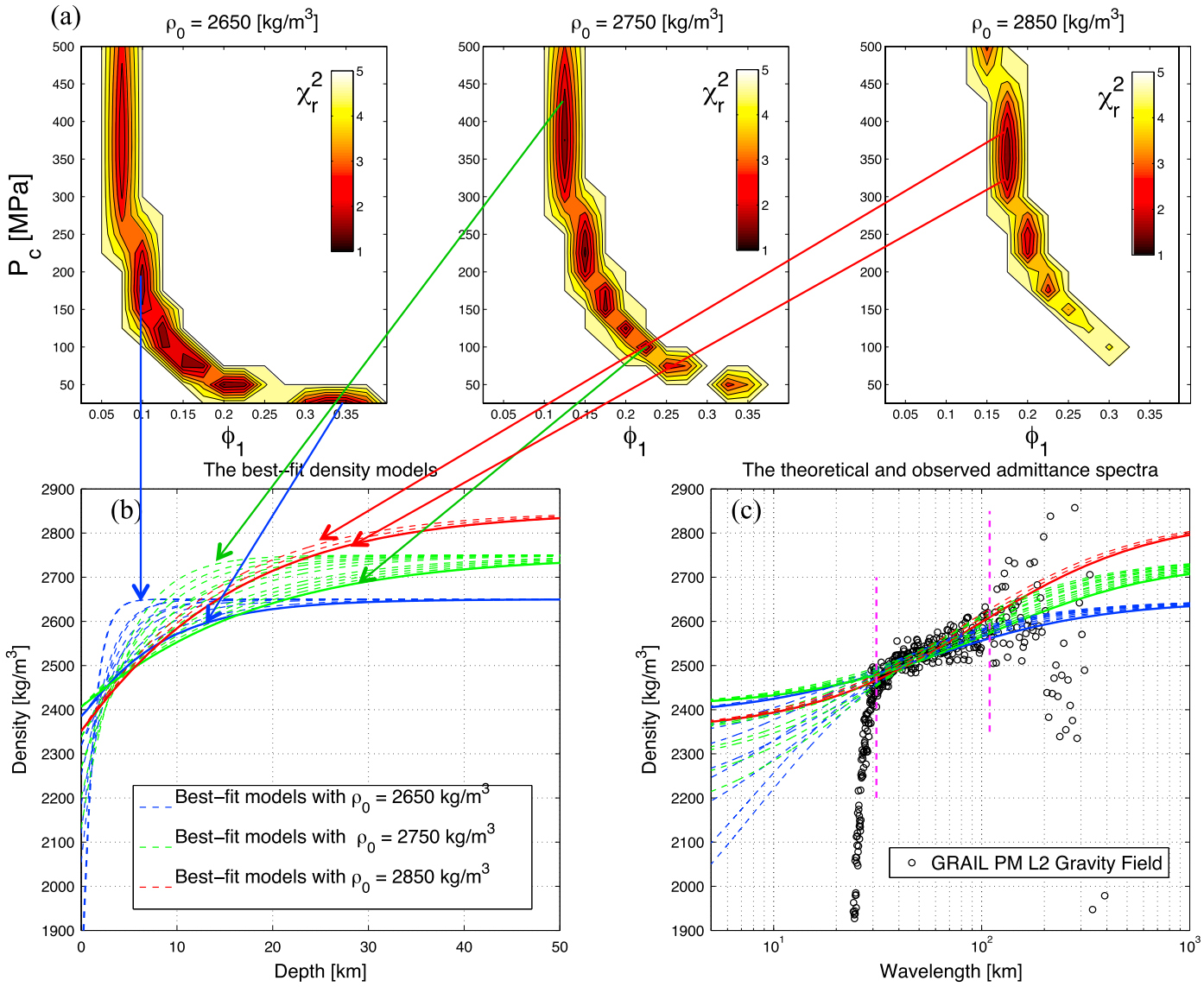

Figure 4. (a) Reduced chi-square statistics (χ_r^2) illustrating goodness of the fit between the GRAIL admittance observation (Figure 1b) and the theoretical admittance for various cases of crustal density stratification with a range of ρ_0, ϕ_1, and P_c. The models yielding $\chi_r^2 < 2$ fit the observed admittance within the uncertainty of 25 kg/m^3. (b) The depth-density models found for the case of ρ_0 = 2650, 2750, and 2850 kg/m^3. The solid line in each ρ_0 indicates the solution with gradually increasing (smaller gradient) density with depth over 10–20 km. (c) The observed and theoretical admittance spectra from GRAIL and the best fit models.

20 km owes to high-frequency dampening applied in the GRAIL gravity field solutions [*Konopliv et al.* 2013; *Lemoine et al.* 2013]. The crustal gravity model with the uniform density of 2550 kg/m^3 does not sufficiently fit the GRAIL gravity field, particularly over the wavelengths of 30–50 km. The gravity models with the stratified density structures show improved agreement with the GRAIL gravity field, presenting smaller Bouguer coherence.

We also examined a week (21–27 November 2012) of Level-1B (L1B) data from the GRAIL XM, where the higher spatial resolution of gravity information is expected due to the lowered altitude of spacecrafts. We used the L1B intersatellite ranging data along with the orbit data to process the line of sight gravity difference and computed the Bouguer coherence spectrum following the method of *Han* [2013]. The free-air coherence spectrum shows the unity value extended to 20 km or so, confirming the higher sensitivity of the XM data. Over 20–50 km, it is also evident that the crustal models with the density stratification fit the GRAIL L1B data better and give the smaller Bouguer coherence than the uniform density model.

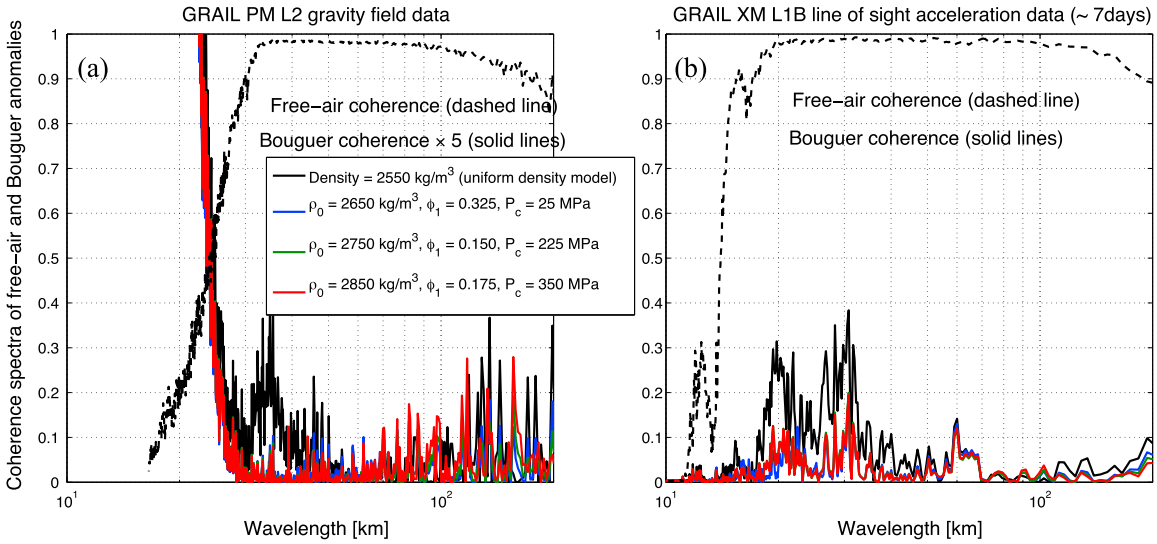

Figure 5. (a) The free-air and Bouguer coherence spectra from the GRAIL primary mission (PM) global gravity field data and (b) from the GRAIL XM intersatellite line of sight gravity difference data for a week. The results from the synthetic gravity fields with the stratified density models (color lines) and with the uniform density of 2550 kg/m^3 (black line) are compared. In both PM and XM data, the smaller Bouguer coherence is found with the stratified density models, being particularly evident over the short wavelength band (30–50 km for PM L2 data and 20–50 km for XM L1B data). It indicates that the GRAIL gravity data agree better with the synthetic gravity models computed using the stratified density.

5. Summary and Discussion

The GRAIL high-precision data indicate that the gravity response to topography decreases systematically from 100 km down to 30 km wavelengths, while the correlation between the two fields by degree stays close to unity. The gravity signal at the wavelength of 30 km is accounted for by the crustal density of 2450 kg/m^3 that is 100 kg/m^3 smaller than the density required at 100 km. It is more evident in the recent study with the preliminary XM gravity fields by *Wieczorek et al.* [2013b]. To explain such wavelength-dependent characteristics, we introduced a simple, experimental model of compaction of sedimentary rocks that relates porosity (or density) and depth in a convenient way [*Athy*, 1930; *Audet and Fowler*, 1992]. Our modeling result supports the assertion that the crustal density may vary widely from surface to deep crust by up to 500 kg/m^3 satisfying the GRAIL observation of high-resolution gravity in conjunction with LOLA topography data.

With the constraint on the surface bulk density near 2400 kg/m^3, our compaction model found that the porosity decreases exponentially with depth within the 10–20 km thick (porous) layers depending on the grain density between 2600 and 2900 kg/m^3. The surface porosity is determined from 0.10 to 0.17 for the lower and upper bound of the grain density, respectively. They are comparable to the layer thickness and porosity determined by *Wieczorek et al.* [2013a]. Another possible stratification model is found with the lower bound (2600 kg/m^3). In this model, a large surface porosity of 0.30–0.35 in a thin porous layer limited to the top 3 km satisfies the GRAIL observations within the wavelength band of 30–100 km, beyond which the interior geophysical processes and data noise hamper our analysis. Both models provide improved predictions of the high-frequency components of the lunar gravity field, yielding a smaller Bouguer coherence than the uniform density crustal model.

A recent reappraisal by *Kiefer et al.* [2012] of porosity and density in Apollo samples and meteorites that spanned a wide range of lunar crustal materials found that samples of the feldspathic highland crust had densities of 2200–2600 kg/m^3 and porosities of 10–20%, while the ejecta associated with impact basins had a bulk density of 2350–2600 kg/m^3 and a porosity of ~20%. This range favors our class of material models with higher grain density (2800–2900 kg/m^3) and closure pressures (200–250 MPa), suggesting that porosity could extend 10–20 km within the lunar crust. This observation is also commensurate with lowered seismic velocities extending into the uppermost 10–20 km of the lunar crust [e.g., *Nakamura*, 1983; *Lognonné et al.*, 2003; *Khan et al.*, 2013].

The basic feature of density stratification reported in this study is a first-order global characteristic of the lunar crust. While our modeling only considers overburden pressure for pore space closure, viscous deformation alongside thermal evolution also presents a viable mechanism for yielding a depth-dependent porosity and

density [*Nimmo et al.*, 2003; *Besserer et al.*, 2014]. The lunar crust will most likely exhibit strong lateral heterogeneity in density (both porosity and composition) given its complex history of impact bombardment and volcanism. In addition to changes in density, changes in porosity will affect seismic wave velocities [*Sondergeld et al.*, 1979] and thermal conductivity of the lunar megaregolith [*Binder and Lange*, 1980]. The lateral heterogeneity in crustal porosity may also lead to large variations in thermal conductivity through the megaregolith layer, leading to different thermal histories across lunar terrains [e.g., *Ziethe et al.*, 2009; *Zhang et al.*, 2013]. The local and integrated analysis of high-resolution gravity, topography, seismic, and other remote sensing data to comprehensively characterize the lunar crust is necessary to improve our knowledge on surface process, interior structure, and modification by geologic processes of the Moon.

Acknowledgments

This work was supported by NASA's LASER program and GRACE projects. We gratefully appreciate the GRAIL principal investigators and their team for releasing the L1B and L2 data within 6 months after the end of the primary mission. We thank Walter Kiefer and an anonymous reviewer for reviewing this paper.

The Editor thanks Walter Kiefer and an anonymous reviewer for their assistance in evaluating this paper.

References

Athy, L. F. (1930), Density, porosity, and compaction of sedimentary rocks, *AAPG Bull.*, *14*, 1–24.

Audet, D., and A. Fowler (1992), A mathematical model for compaction in sedimentary basins, *Geophys. J. Int.*, *110*, 577–590.

Besserer, J., F. Nimmo, M. A. Wieczorek, R. C. Weber, W. S. Kiefer, P. J. McGovern, D. E. Smith, and M. T. Zuber (2014), GRAIL constraints on the vertical density structure of the lunar crust, Abstract #2407, paper presented at 45th Lunar and Planetary Science Conference, Houston, Tex.

Binder, A. B., and M. A. Lange (1980), On the thermal history, thermal state, and related tectonism of a Moon of fission origin, *J. Geophys. Res.*, *85*(B6), 3194–3208, doi:10.1029/JB085iB06p03194.

Han, S.-C. (2013), Determination and localized analysis of intersatellite line of sight gravity difference: Results from the GRAIL primary mission, *J. Geophys. Res. Planets*, *118*, 2323–2337, doi:10.1002/2013JE004402.

Hartmann, W. K. (1973), Ancient lunar mega-regolith and subsurface structure, *Icarus*, *18*, 634–636.

Heck, B., and K. Seitz (2007), A comparison of the tesseroid, prism and point-mass approaches for mass reductions in gravity field modeling, *J. Geodesy*, *81*, 121–136, doi:10.1007/s00190-006-0094-0.

Keihm, S. J., and M. G. Langseth (1977), Lunar thermal regime to 300 km, *Proc. Lunar Planet. Sci. Conf.*, *8*, 499–514.

Khan, A., A. Pommier, G. A. Neumann, and K. Mosegaard (2013), The lunar moho and the internal structure of the Moon: A geophysical perspective, *Tectonophysics*, *609*, 331–352, doi:10.1016/j.tecto.2013.02.024.

Kiefer, W. S., R. J. Macke, D. T. Britt, A. J. Irving, and G. J. Consolmagno (2012), The density and porosity of lunar rocks, *Geophys. Res. Lett.*, *39*, L07201, doi:10.1029/2012GL051319.

Konopliv, A. S., et al. (2013), The JPL lunar gravity field to spherical harmonic degree 660 from the GRAIL Primary Mission, *J. Geophys. Res. Planets*, *118*, 1415–1434, doi:10.1002/jgre.20097.

Lemoine, F. G., et al. (2013), High-degree gravity models from GRAIL primary mission data, *J. Geophys. Res. Planets*, *118*, 1676–1698, doi:10.1002/jgre.20118.

Lognonné, P., J. Gagnepain-Beyneix, and H. Chenet (2003), A new seismic model of the Moon: Implications for structure, thermal evolution and formation of the Moon, *Earth Planet. Sci. Lett.*, *211*, 27–44.

Nakamura, Y. (1983), Seismic velocity structure of the lunar mantle, *J. Geophys. Res.*, *88*, 677–686.

Nakamura, Y. (2011), Timing problem with the Lunar Module impact data as recorded by the LSPE and corrected near-surface structure at the Apollo 17 landing site, *J. Geophys. Res.*, *116*, E12005, doi:10.1029/2011JE003972.

Nimmo, F., R. T. Pappalardo, and B. Giese (2003), On the origins of band topography, Europa, *Icarus*, *166*, 21–32, doi:10.1016/j.icarus.2003.08.002.

Sclater, J. G., and P. A. F. Christie (1980), Continental stretching: An explanation of the Post-Mid-Cretaceous subsidence of the central North Sea Basin, *J. Geophys. Res.*, *85*, 3711–3739.

Smith, D. E., et al. (2010), Initial observations from the Lunar Orbiter Laser Altimeter (LOLA), *Geophys. Res. Lett.*, *37*, L18204, doi:10.1029/2010GL043751.

Sondergeld, C. H., L. A. Granryd, and H. A. Spetzler (1979), Compressional velocity measurements for a highly fractured lunar anorthosite, *Proc. Lunar Planet Sci. Conf.*, *10*, 1143–1145.

Töksoz, M. N., A. M. Dainty, S. C. Solomon, and K. R. Anderson (1974), Structure of the Moon, *Rev. Geophys.*, *12*, 539–567.

Turcotte, D. L., R. J. Willemann, W. F. Haxby, and J. Norberry (1981), Role of membrane stresses in the support of planetary topography, *J. Geophys. Res.*, *86*, 3951–3959.

Wieczorek, M. A., and R. J. Phillips (1998), Potential anomalies on a sphere: Applications to the thickness of the lunar crust, *J. Geophys. Res.*, *103*, 1715–1724, doi:10.1029/97JE03136.

Wieczorek, M. A., et al. (2013a), The crust of the Moon as seen by GRAIL, *Science*, *339*, 671–675, doi:10.1126/science.1231530.

Wieczorek, M. A., et al. (2013b), High-resolution estimates of lunar crustal density and porosity from the GRAIL extended mission, Abstract #1914, paper presented at 44th Lunar and Planetary Science Conference, Houston, Tex.

Wieczorek, M. A. (2008), Constraints on the composition of the Martian south polar cap from gravity and topography, *Icarus*, *196*, 506–517, doi:10.1016/j.icarus.2007.10.026.

Zhang, N., E. M. Parmentier, and Y. Liang (2013), Effects of lunar cumulate mantle overturn and megaregolith on the expansion and contraction history of the Moon, *Geophys. Res. Lett.*, *40*, 5019–5023, doi:10.1002/grl.50988.

Ziethe, R., K. Seiferlin, and H. Hiesinger (2009), Duration and extent of lunar volcanism: Comparison of 3D convection models to mare basalt ages, *Planet. Space Sci.*, *57*, 784–796.

Zuber, M. T., et al. (2013), Gravity field of the Moon from the Gravity Recovery and Interior Laboratory (GRAIL) mission, *Science*, *339*, 668–671, doi:10.1126/science.1231507.